Advanced Simulation of Conductance Histograms Validated through Channel-Sensitive Experiments on Indium Nanojunctions

P. Makk,[1] D. Visontai,[2] L. Oroszlány,[3] D. Zs. Manrique,[2] Sz. Csonka,[1] J. Cserti,[3] C. Lambert,[2] and A. Halbritter[1]

[1]*Department of Physics, Budapest University of Technology and Economics and Condensed Matter Research Group of the Hungarian Academy of Sciences, 1111 Budapest, Budafoki ut 8., Hungary*

[2]*Department of Physics, Lancaster University, Lancaster LA1 4YB, United Kingdom*

[3]*Department of Physics of Complex Systems, Eötvös University, H-1117 Budapest, Pázmány Péter sétány 1/A, Hungary*

(Received 26 July 2011; published 28 December 2011)

We demonstrate a self-contained methodology for predicting conductance histograms of atomic and molecular junctions. Fast classical molecular-dynamics simulations are combined with accurate density functional theory calculations predicting both quantum transport properties and molecular-dynamics force field parameters. The methodology is confronted with experiments on atomic-sized indium nanojunctions. Beside conductance histograms the distribution of individual channel transmission eigenvalues is also determined by fitting the superconducting subgap features in the *I-V* curves. The remarkable agreement in the evolution of the channel transmissions demonstrates that the simulated ruptures are able to reproduce a realistic statistical ensemble of contact configurations, whereas simulations on selected ideal geometries show strong deviations from the experimental observations.

DOI: 10.1103/PhysRevLett.107.276801 PACS numbers: 73.63.Rt, 07.05.Tp, 74.45.+c, 81.07.Nb

Nanostructures, in which the current flows through single atoms or single molecules, are ideal test systems to demonstrate the behavior of matter at the ultimate atomic size limit for potential electronic applications. Experimentally, such tiny structures can be constructed using various approaches, including break junction techniques, where an atomic-scale junction is created during the controlled mechanical elongation of a metallic wire [1,2]. In the most common experiment the evolution of the conductance is monitored during the repeated opening and closing of the nanojunction, and the captured conductance-versus-electrode-separation traces are analyzed by conductance histograms [1,2]. Peaks in the histogram reflect the conductance of stable, frequently occurring atomic-scale junction configurations. To gain more information, conductance histograms can be supplemented by the study of nonlinear features in the *I-V* characteristics of the junction [3,4], noise measurements [5], or more advanced statistical analysis of the conductance traces [6]. In all these measurements it is a fundamental ingredient to respect the stochastic nature of nanocontact formation dynamics, and accordingly to perform experiments on a broad statistical ensemble of junctions.

To draw a more complete microscopic picture, all these experimental inputs should be compared with the results of theoretical calculations. Atomic-sized or molecular nanojunctions are commonly described by *ab initio* simulations based on density functional theory (DFT) [2]. However, the computational resources of fully DFT-based simulations of rupture dynamics [7] are highly demanding, therefore DFT calculations are most commonly restricted to the study of a small number of selected ideal geometries, which are chosen to match the presumably most probable experimental contact configurations [8,9]. To better describe the stochastic nature of contact formation and to catch the statistically relevant features, it is desirable to simulate a large statistical ensemble of contact ruptures. For this a proper combination of fast classical molecular-dynamics (MD) simulations [10–12] with precise quantum mechanical calculations of the conductance may provide a reasonable compromise. Recently, a detailed analysis of theoretical conductance histograms was performed, utilizing simpler tight-binding parametrizations of the underlying mean-field Hamiltonian [13,14]. In this case, molecular-dynamics force fields were calculated using semiempirical potentials derived from effective medium theory, whereas tight-binding parameters were obtained from a different approach by fitting to the band structures of bulk materials. Such an approach is reasonable, provided bulk parameters can be transferred to nanojunctions, where many properties are determined by atoms on surfaces or in other low-symmetry positions. Since this pioneering work theoretical conductance histograms were not yet implemented in the field of molecular electronics.

In what follows, we demonstrate a methodology for predicting conductance histograms and other statistical properties, which combines the best features of the above approaches. A statistical ensemble of contact ruptures is simulated by classical MD calculations, and afterwards the underlying mean-field Hamiltonian is evaluated for all the contact configurations by DFT using the local density approximation. The calculations are performed by the SIESTA code [15]. To provide a self-contained method the force field parameters of the MD simulations are obtained by fitting to the results of the DFT calculations for some

model geometries. Finally, the conductance of all the configurations is calculated by a Green's function based evaluation of the Landauer formula $G = (2e^2/h)\sum_i \tau_i$ [16,17], where τ_i represents the transmission probabilities for the conductance eigenchannels of the contact.

We validate the methodology by performing a combined theoretical and experimental analysis of indium nanojunctions, taking advantage of the superconducting phase transition of In at $T = 3.41$ K. In the superconducting phase, multiple Andreev reflections give rise to distinct subgap features in the I-V characteristics of the nanocontact, from which all the transmission probabilities of the conductance eigenchannels of the junction τ_i can be precisely determined [18–20]. The experimental insight to the statistical distribution of the individual channel transmission eigenvalues provides a unique possibility for a strict confrontation of theoretical simulations with reality, going far beyond the comparison of measured and calculated single-atom conductances.

The details of the experimental and theoretical methods are available in the Supplemental Material [21].

Figure 1 demonstrates both experimentally measured and theoretically simulated conductance traces and histograms. Figures 1(a) and 1(b), respectively, show examples of experimental conductance traces and the conductance histogram constructed from 5000 individual traces. The experimental histogram shows a sharp peak at $G \approx 1.1G_0$ ($G_0 = 2e^2/h$), a smaller peak at $G \approx 1.7G_0$, and two broader peaks at $G \approx 2.5G_0$ and $4G_0$, respectively. These peak positions are reproducible for different samples with some variation of the relative peak amplitudes. The theoretical histogram in Fig. 1(d) is constructed from 100 independent simulated conductance traces, from which examples are presented in Fig. 1(c). The simulated histogram nicely reproduces the first peak of the experimental histogram, and it also shows recognizable peaks at higher conductances around 2.5 and $4G_0$, close to the third and fourth experimental peak. The second experimental peak may be reflected by a shoulder around $G \approx 1.5$ in the simulated histogram. The simulated traces show clear conductance plateaus, however, in contrast to the sharp experimental conductance jumps the calculated traces exhibit smoother transition between the plateaus. The conductance steps are mainly governed by the delicate balance of elastic deformation and the change of surface energy. In our view realistic elastic forces are accurately simulated, whereas a proper simulation of surface energy is highly demanding within classical MD simulations. Therefore, the simulations are expected to be precise once a stable configuration is established, but the simulation of the jumps between metastable configurations is less accurate. The agreement with the measured conductance histogram indicates that the simulations are able to provide a realistic ensemble of junction configurations, however, for a stronger justification of this statement a more detailed

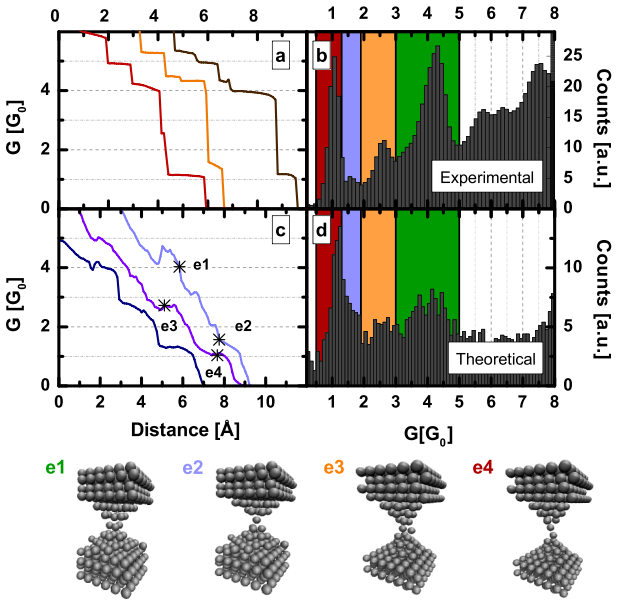

FIG. 1 (color online). The top panels show demonstrative experimental conductance traces (a) and the conductance histogram (b) for indium junctions. The counts are normalized to the number of traces included. The bottom panels show examples of simulated conductance traces (c) and a theoretical conductance histogram (d). Note, that in (a) and (c) the zero point of the distance scale is arbitrarily chosen as the origin of the horizontal axis. Below the panels some atomic configurations are demonstrated (e1)–(e4), respectively, corresponding to the positions on the simulated traces signed by stars.

confrontation of the experimental and theoretical data is necessary.

For a deeper comparison of the simulated data with experimental junction configurations we perform a detailed statistical analysis of the conductance channels' transmission eigenvalues. Experimentally we have measured the current-voltage characteristics of more than 500 independent junctions in the superconducting state, and by fitting the subgap structures we have determined the transmission probabilities τ_i for the open conductance channels of all these junctions [21]. The channel transmissions are also determined along all points of the simulated 100 traces by diagonalizing $t^\dagger t$, where t is the transmission part of the scattering matrix.

Experimentally we have found that in spite of the stochastic nature of contact rupture the evolution of the average channel transmissions as a function of the total conductance is material specific, and it is a well-defined function for a given material. This evolution is demonstrated in Fig. 2 both for the measurements on In junctions and for the simulations (orange squares and blue circles, respectively). A remarkable agreement is found between theory and experiment, which gives a strong justification that the simulations provide a realistic ensemble of

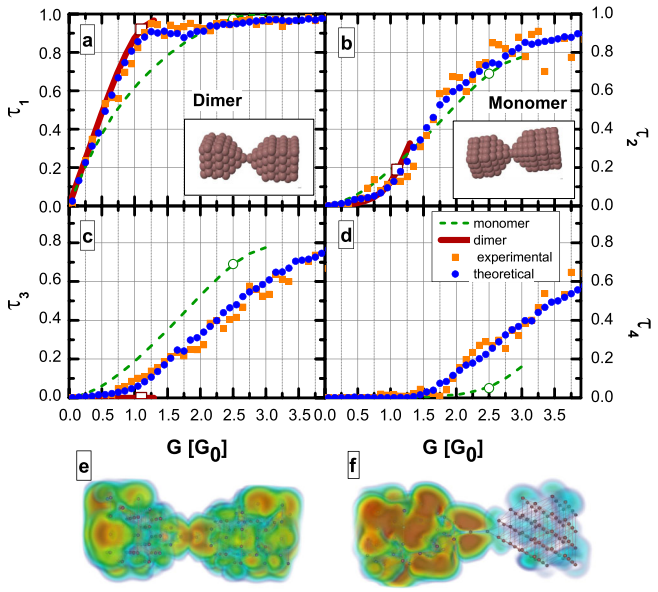

FIG. 2 (color online). (a)–(d) The orange squares and blue circles, respectively, show the mean value of the experimental and theoretical channel transmissions. The solid red (dashed green) lines, respectively, show the channel transmissions during the stretching of an ideal dimer (monomer) configurations. The geometries of these ideal configurations are demonstrated in the insets. Panels (e) and (f) demonstrate the scattering wave function of the first two eigenchannels in a junction with an ideal dimer configuration ($G = 1.18G_0$, $\tau_1 = 0.985$, $\tau_2 = 0.102$). The first channel (e) shows a σ-type, whereas the second channel (f) shows a π-type wave function at the central two atoms.

junction configurations. The complete distribution of measured and calculated transmission eigenvalues is demonstrated in the Supplemental Material [21].

This agreement allows us to identify the typical atomic configurations, which are responsible for the different peaks in the experimental histogram. After a detailed analysis of the atomic arrangements along the theoretical conductance traces, we have found a clear matching between the four distinct conductance regions around the peak positions [four color areas in Figs. 1(b) and 1(d)] with some typical contact configurations demonstrated in Figs. 1(e1)–(e4). The region of the fourth peak ($G = 3$–$5G_0$, green area) is typically related to configurations with 3 or 4 atoms in the smallest cross section [Fig. 1(e1)], which we denote by N-3-N' or N-4-N' configuration (the middle number is the number of atoms in the smallest cross section, whereas N and N' are the number of neighbor atoms on both sides which can have different values being larger than the middle number). The third peak ($G = 1.9$–$3G_0$, orange area) basically corresponds to arrangements with 2 atoms in the smallest cross section [N-2-N' configuration, Fig. 1(e3)]. The small peak at $G \approx 1.7G_0$ ($G = 1.3$–$1.9G_0$, blue area) is mainly related to a monomer configuration with a single atom in the smallest cross section [N-1-N', Fig. 1(e2)]. The position of the first peak ($G = 0.5$–$1.3G_0$, red area) is clearly related to a dimer configuration, where a chain of two atoms connects the two electrodes [N-1-1-N', Fig. 1(e4)]. A movie demonstrating the evolution of the contact configuration along the simulated conductance traces is available in the Supplemental Material [21].

Until now, most of the DFT-based calculations were applied to small numbers of selected geometries and therefore for comparison, we have performed simulations on some ideal pyramidlike junctions, which are cleaved from bulk indium crystal structure without any relaxation. The solid (red) lines in Fig. 2 demonstrate the opening of the conductance channels as the distance between the apex atoms of an ideal {001}-oriented dimer configuration is varied [the ideal geometry is demonstrated in the inset of Fig. 2(a)]. At the optimized separation, the conductance of the ideal dimer configuration is $G \approx 1G_0$ (red square), in agreement with the simulated traces [e.g. Fig. 1(e4)]. The transmission probabilities of the first two channels for this geometry show reasonable agreement with the experiment, whereas the almost zero transmission of the third channel is far below the experimental data. As a second example, the dashed (green) curve shows the opening of the conductance channels for an ideal {001}-oriented monomer configuration [see inset of Fig. 2(b)]. For this arrangement the conductance at the optimal separation is $G \approx 2.5G_0$ (green circle), which significantly exceeds the conductance of monomer configurations obtained by MD simulations, and furthermore the evolution of the channel transmissions strongly deviate from the experimental mean values. These discrepancies are attributed to the sensitivity to the number of neighbor atoms, which is defined to be 2×4 for the ideal monomer, whereas in the MD-based traces the middle atom usually has only 2 or 3 neighbors on each contact. The above comparisons demonstrate, that at $G < 1.1G_0$ the junctions are reasonably described by an ideal dimer configuration, although the transmission probabilities show deviations from the experiment presumably due to the unrealistic symmetry of the ideal structure. However, at higher conductances, where the precise geometry of the junction strongly influences the conductance, ideal configurations give a false result, and besides the simulations of ideal geometries are not able to describe transitions between different configurations. In contrast, MD simulations are able to sort out the statistically relevant ensemble of configurations, and can provide excellent agreement with the experimental data even on the level of individual channel transmissions.

With theoretical simulations not only the transmission probabilities, but also the scattering wave functions corresponding to the different conductance channels can be determined. Figures 1(e) and 1(f) show the absolute value of the wave functions of the first two eigenchannels of an ideal dimer configuration, associated with an incoming

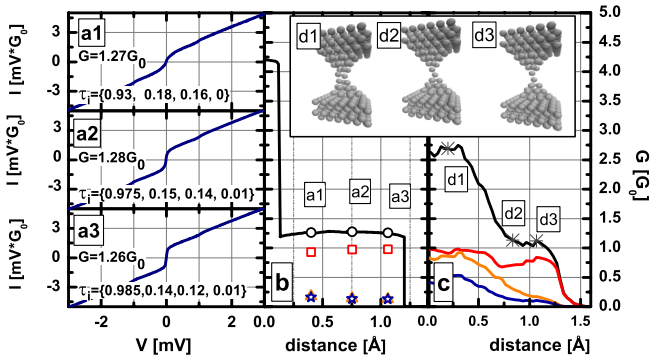

FIG. 3 (color online). An experimentally measured conductance plateau (b) and the *I*-*V* curves recorded at three different points of the plateau (a1)–(a3). The fitted channel transmissions are given in the insets of panels (a1)–(a3), and demonstrated by red squares, blue stars, and orange triangles in panel (b) Panel (c) demonstrates a theoretical conductance trace (top black curve) together with the evolution of the channels transmissions (lower three curves, red, orange, and blue, respectively). Panels (d1)–(d3) demonstrate the junction geometries at the three points of the theoretical trace marked by stars.

wave from the left electrode. It is clear that the first, highly transmitting channel is related to a σ-type, whereas the second channel with significantly smaller transmission is related to a π-type wave function on the central two atoms. This picture agrees with previous tight-binding calculations, which have shown that in p metals, the first channel comes from the hybridization of s and p_z orbitals, whereas the second and third channels are related to p_x and p_y orbitals [22].

It is also interesting to follow the evolution of the conductance channels along individual conductance plateaus. Figure 3(b) shows a rather flat conductance plateau in the region of the first histogram peak. The channel transmissions were measured at three points on the conductance plateau (black circles). The total conductance of these points is constant with an accuracy of 1.5%. In contrast, during stretching the transmission of the first channel increases with more than 5% towards unity [as demonstrated by the enhancement of the zero bias supercurrent in the *I*-*V* curves, Fig. 3(a1)–(a3)] and the transmissions of the further channels decrease. We have found this type of behavior (i.e., the opening of the first channel as the junctions is stretched along a straight plateau) rather typical in indium junctions, which was frequently observed in theoretical simulations as well [Fig. 3(c)]. According to the simulations, this behavior has a geometrical origin; the final stage of the rupture is frequently associated with a dimer contact tilting towards the contact axis [Fig. 3(d1)–(d3)]. During this process the σ-type channel is found to have the largest transmission at the final, most symmetric configuration (dimer parallel with the axis), whereas the transmission through the π-type channels is gradually suppressed. For further illustration, the evolution of the wave functions along this conductance trace is demonstrated by a video in the Supplemental Material [21].

In conclusion, we have demonstrated a self-contained method for the simulation of a statistical ensemble of junction configurations and conductance histograms. To obtain a proper compromise between speed and accuracy we have combined DFT-based calculations of the conductance with classical MD simulations of the rupture. The MD force fields were fitted to DFT calculations, which ensures the self-contained nature of the method, and enables its application for a wide range of materials—including multicomponent systems—without a detailed *a priori* knowledge of material properties. The simulations were confronted with experiments on indium nanojunctions. Experimentally not only were conductance traces and conductance histograms measured, but also a detailed insight into the distribution of individual channel transmission eigenvalues was obtained by fitting the subgap structures in the *I*-*V* curves of a statistical amount of superconducting junctions. The simulations have shown remarkable agreement with experiment even on the level of individual transmission eigenvalues, demonstrating that the classical MD simulations are able to produce a realistic ensemble of junction configurations. However, if the contact rupture is not simulated by MD, rather the conductance is calculated along the elongation of some ideal contact configurations a strong deviation is obtained from the experimental data. This comparison demonstrates that ideal structures—which are frequently adopted in simulations—are not realistic representations of experimental junctions, and a statistical approach is essential for an accurate identification of typical experimental junction configurations.

The proposed statistical approach would also improve the outcome of simulations on single-molecule junctions and other molecular electronics devices, where stochasticity is a major experimental difficulty. The force-field parametrization of multicomponent systems is not uncommon in MD calculations [23–27], and DFT level conductance calculations are also routinely performed on molecular junctions. Utilizing these experiences our combined approach could indeed be generalized to systems containing multiple atomic species.

The authors are grateful to J. Ferrer, M. Migliorato, and J. Jefferson for fruitful discussions and to G. Rubio-Bollinger for the multiple Andreev reflection fitting code. This work has been supported by the Hungarian research funds No. OTKA K76010, No. K75529, No. NK72916, No. NNF78842, No. TAMOP-4.2.1/B- 09/1/KMR-2010-0002, No. TÁMOP 4.2.1./B-09/1/KMR-2010-0003, and the EU Grants NanoCTM and FUNMOLS, ERG 239223. A. H. and S. C. received support from a Bolyai János Scholarship.

[1] N. Agraït, A. Levy Yeyati, and J. M. van Ruitenbeek, Phys. Rep. **377**, 81 (2003).
[2] J. C. Cuevas and E. Scheer, *Molecular Electronics: An Introduction to Theory and Experiment* (World Scientific Publishing Company, Singapore, 2010).
[3] A. Halbritter *et al.*, Phys. Rev. B **77**, 075402 (2008).
[4] R. H. M. Smit *et al.*, Nature (London) **419**, 906 (2002).
[5] D. Djukic and J. M. van Ruitenbeek, Nano Lett. **6**, 789 (2006).
[6] A. Halbritter *et al.*, Phys. Rev. Lett. **105**, 266805 (2010).
[7] M. Paulsson *et al.*, Nano Lett. **9**, 117 (2009).
[8] M. Strange, K. S. Thygesen, and K. W. Jacobsen, Phys. Rev. B **73**, 125424 (2006).
[9] V. M. García-Suárez, D. Z. Manrique, C. J. Lambert, and J. Ferrer, Phys. Rev. B **79**, 060408 (2009).
[10] U. Landman *et al.*, Science **248**, 454 (1990).
[11] M. R. Sørensen, M. Brandbyge, and K. W. Jacobsen, Phys. Rev. B **57**, 3283 (1998).
[12] P. García-Mochales *et al.*, Nanotechnology **19**, 225704 (2008).
[13] M. Dreher *et al.*, Phys. Rev. B **72**, 075435 (2005).
[14] F. Pauly *et al.*, Phys. Rev. B **74**, 235106 (2006).
[15] J. M. Soler *et al.*, J. Phys. Condens. Matter **14**, 2745 (2002).
[16] A. R. Rocha *et al.*, Nature Mater. **4**, 335 (2005).
[17] A. R. Rocha *et al.*, Phys. Rev. B **73**, 085414 (2006).
[18] J. C. Cuevas, A. Martín-Rodero, and A. Levy Yeyati, Phys. Rev. B **54**, 7366 (1996).
[19] J. J. Riquelme *et al.*, Europhys. Lett. **70**, 663 (2005).
[20] E. Scheer *et al.*, Nature (London) **394**, 154 (1998).
[21] See Supplemental Material at http://link.aps.org/supplemental/10.1103/PhysRevLett.107.276801 for a detailed description of the experimental and theoretical methods, and for two supplementing videos of the simulation results.
[22] J. C. Cuevas, A. Levy Yeyati, and A. Martín-Rodero, Phys. Rev. Lett. **80**, 1066 (1998).
[23] D. Powell *et al.*, Physica (Amsterdam) **32E**, 270 (2006).
[24] Q. Pu *et al.*, J. Phys. Chem. C **114**, 10365 (2010).
[25] L. Dai *et al.*, Langmuir **26**, 1165 (2010).
[26] K. Tay and F. Bresme, J. Mater. Chem. **16**, 1956 (2006).
[27] J. T. Titantah *et al.*, J. Appl. Phys. **101**, 123508 (2007).